JOURNAL OF AGRICULTURAL AND FOOD CHEMISTRY

pubs.acs.org/JAFC Article

Schisandrin B Promotes Hepatic Stellate Cell Ferroptosis via Wnt Pathway-Mediated Ly6C^{lo} Macrophages

Xinmiao Li, Feng Jiang, Yuhang Hu, Zhichao Lang, Yating Zhan, Rongrong Zhang, Qiqi Tao, Chengchu Luo, Jinglu Yu, and Jianjian Zheng*

Cite This: *J. Agric. Food Chem.* 2023, 71, 17295−17307 Read Online

ACCESS | Metrics & More | Article Recommendations | Supporting Information

ABSTRACT: A key event in liver fibrosis is the activation of the hepatic stellate cell (HSC). Schisandrin B (Sch B), a major component extracted from *Schisandra chinensis*, has been shown to inhibit HSC activation. Recently, ferroptosis (FPT) has been reported to be involved in HSC activation. However, whether Sch B has an effect on the HSC FPT remains unclear. Herein, we explored the effects of Sch B on liver fibrosis *in vivo* and *in vitro* and the roles of Wnt agonist 1 and ferrostatin-1 in the antifibrotic effects of Sch B. Sch B effectively alleviated CCl_4-induced liver fibrosis, with decreased collagen deposition and α-SMA level. Additionally, Sch B resulted in an increase in lymphocyte antigen 6 complex locus C low (Ly6C^{lo}) macrophages, contributing to a reduced level of TIMP1 and increased MMP2. Notably, the Wnt pathway was involved in Sch B-mediated Ly6C macrophage phenotypic transformation. Further studies demonstrated that Sch B-treated macrophages had an inhibitory effect on HSC activation, which was associated with HSC FPT. GPX4, a negative regulator of FPT, was induced by Sch B and found to be involved in the crosstalk between macrophage and HSC FPT. Furthermore, HSC inactivation as well as FPT induced by Sch B-treated macrophages was blocked down by Wnt pathway agonist 1. Collectively, we demonstrate that Sch B inhibits liver fibrosis, at least partially, through mediating Ly6C^{lo} macrophages and HSC FPT. Sch B enhances Wnt pathway inactivation, leading to the increase in Ly6C^{lo} macrophages, which contributes to HSC FPT. Sch B may be a promising drug for liver fibrosis treatment.

KEYWORDS: *Schisandrin B, macrophages, Ly6C, ferroptosis, liver fibrosis*

INTRODUCTION

Liver fibrosis is the result of chronic liver injury, often progressing to cirrhosis and liver failure if not controlled.[1] Liver fibrosis is distinguished by the accumulation of the extracellular matrix (ECM) and a heightened collagen fiber level. Generally, liver fibrosis is associated with a persistent inflammatory reaction. Liver ECM proteins are mainly produced by activated hepatic stellate cells (HSCs), which can be triggered by pro-inflammatory stimuli.[2] Therefore, inhibition of HSC activation and/or pro-fibrotic cytokines is a viable option to alleviate liver fibrosis.

It is known that macrophages act as major mediators in organ fibrosis development.[3] Recently, macrophages have been shown to be associated with HSC activation.[4] In addition, according to the expression of a surface marker, the lymphocyte antigen 6 complex locus C (Ly6C),[5] liver macrophages could be divided into two subsets: Ly6C is high (Ly6C^{hi}) and Ly6C is low (Ly6C^{lo}). Ly6C^{hi} macrophages have been demonstrated to be pro-inflammatory and pro-fibrotic, while Ly6C^{lo} macrophages have the potential to reduce inflammation and facilitate fibrosis degradation.[6] Moreover, Ly6C^{hi} macrophages have been shown to be able to release pro-fibrotic factors, including transforming growth factor β (TGF-β) and CCL2 (also known as monocyte chemoattractant protein-1, MCP-1). Notably, CCL2, a chemokine, has been reported to directly activate HSC.[7] Inducible nitric oxide synthase (iNOS) is an enzyme that plays a role in NO synthesis. iNOS expression is absent in resting cells but is induced by immunological stimuli, such as bacterial lipopolysaccharide (LPS).[8] Increasing studies have shown the involvement of iNOS in liver fibrosis.[9] For instance, Hamada et al. previously reported that liver injury could be attenuated in iNOS knockout mice.[10]

Ferroptosis (FPT), discovered in 2012, is a new form of cell death that depends on the regulation of iron and reactive oxygen species (ROS).[11] FPT, apart from other forms of regulated cell death, has been identified to possess distinct features, in terms of its morphology, biochemistry, and genetics. Morphologically, ferroptotic cells display a decreased mitochondrial size, a condensed mitochondrial membrane, a lack of mitochondrial cristae, and even broken outer mitochondrial membranes.[12] Recently, increasing evidence has shown that FPT participates in the progression of human cancers, such as hepatocellular carcinoma (HCC).[13] In addition, FPT has been implicated in liver fibrosis. For example, Zhang et al. revealed that artemether treatment reduces liver fibrosis and inhibits HSC activation by inducing p53-dependent HSC FPT.[14] Therefore, FPT may be a new and effective approach for regulating HSC activation.

Received: May 23, 2023
Revised: October 11, 2023
Accepted: October 19, 2023
Published: November 3, 2023

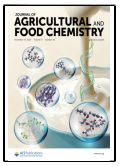

https://doi.org/10.1021/acs.jafc.3c03409
J. Agric. Food Chem. 2023, 71, 17295−17307

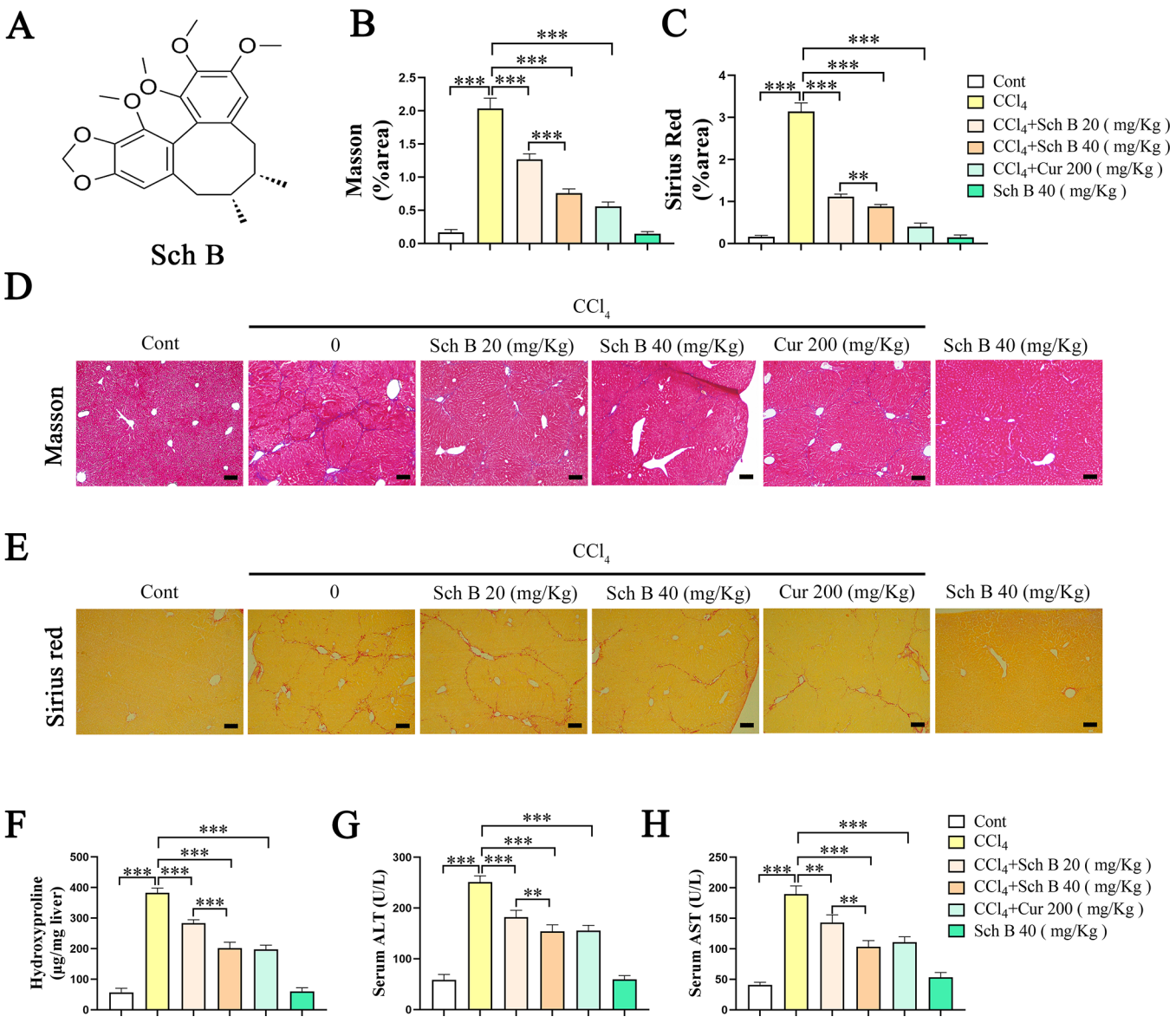

Figure 1. Sch B alleviates CCl_4-induced liver fibrosis *in vivo*. (A) Chemical structure of Sch B. (B−E) Masson staining and Sirius red staining in mice. Scale bars, 100 μm. (F−H) Hyp, ALT, and AST level in mice. Each value is the mean ± SD of six experiments. $^{**}P < 0.01$ and $^{***}P < 0.001$.

Schisandrin B (Sch B) ($C_{23}H_{28}O_6$, molecular weight = 400.46; Figure 1A) is a major component extracted from *Schisandra chinensis*.[15] A previous study has shown that Sch B can relieve liver fibrosis.[16] Sch B has been found to have beneficial effects on liver fibrosis in animal models.[17] In this study, we demonstrated that Sch B inhibits liver fibrosis, at least partially, via the Wnt pathway-mediated $Ly6C^{lo}$ macrophages.

MATERIALS AND METHODS

Materials. Sch B (≥95% purity) and carbon tetrachloride (CCl_4) were obtained from Sigma-Aldrich (St. Louis, MO, USA). Primary antibodies against α-SMA, type I collagen, c-Myc, lymphoid enhancement factor 1 (LEF1), β-actin, iNOS, MCP-1, tissue inhibitor of metalloproteinases 1 (TIMP1), matrix metalloproteinase 2 (MMP2), GPX4, phosphorylation-β-catenin (P-β-catenin), ACSL4, and SLC7A11 were from Abcam (Shanghai, China).

Animal Experiments. This experiment was approved by the Laboratory Animal Ethics Committee of Wenzhou Medical University. Eight week old C57BL/6J mice (n = 6) were used to create the mouse model of liver fibrosis by administering intraperitoneal injections of CCl_4 (Sigma-Aldrich, St. Louis, MO, USA) in olive oil (10%, 7 μL/g) twice a week for 8 weeks. The control group (n = 6) was injected with an equivalent volume of olive oil, while the Sch B group was treated with Sch B (20 mg/kg) (n = 6) or Sch B (40 mg/kg) (n = 6) daily via gavage during the CCl_4 period.[17] The Cur group (n = 6) was administered Cur (200 mg/kg) via gavage. After the experiment, mice were euthanized under anesthesia and blood, bone marrow, and liver tissue samples were collected for further analysis.

Pathological Evaluation of the Liver. Liver tissues were fixed in 10% neutral formalin for 48 h and then underwent dehydration with ethanol, xylene permeation, and paraffin embedding. Sections of 4 μm thickness were cut for Sirius Red staining and Masson staining to evaluate liver fibrosis, which can accurately assess collagen accumulation in fibrotic liver tissues.[18]

Hepatic Hydroxyproline (Hyp) Content. In line with the manufacturer's instructions, the Hyp content in the liver tissue was determined using the Hyp colorimetric assay kit (BioVision, San Francisco, CA). The process included blending the liver tissue with HCl and hydrolyzing it for 12 h followed by centrifuging the lysate at 12,000g at 4 °C for 10 min to obtain the supernatant.

https://doi.org/10.1021/acs.jafc.3c03409
J. Agric. Food Chem. 2023, 71, 17295−17307

Determination of Alanine Aminotransferase (ALT) and Aspartate Aminotransferase (AST) in Serum. Blood samples were spun in a centrifuge at 3000*g* for 10 min. Then, serum samples were evaluated using AST and ALT activity colorimetric assay kits (Rongsheng, Shanghai, China).

Immunohistochemistry. Specimens were fixed in 4% formalin followed by degreasing and rehydration. After blocking with 10% bovine serum albumin, samples were incubated at 4 °C for no less than 12 h with primary antibodies against α-SMA and type I collagen followed by incubation with a horseradish peroxidase-conjugated goat antirabbit IgG secondary antibody for 30 min at room temperature. Finally, the areas marked with α-SMA or type I collagen were further inspected by using a microscope (Carl Zeiss, Germany).

Isolation and Culture of Bone Marrow-Deprived Macrophage (BMDM). BMDMs were obtained as previously described.[19] Cells were collected from the tibiae and femurs of 8 week old C57BL/6 healthy or CCl_4 and Sch B-treated mice. They were then cultivated in Dulbecco's modified Eagle's medium (DMEM, Corning) supplemented with 10% fetal bovine serum (GIBCO) and 1% penicillin−streptomycin (GIBCO). Cells were treated with mouse macrophage colony-stimulating factor (Peprotech) for 6 days to induce differentiation. The population of BMDM was assessed by expression of the F4/80 surface molecule by FACS analysis, and more than 99% pure BMDMs were obtained.

Quantitative Real-Time Polymerase Chain Reaction (qRT-PCR) Analysis. The total RNA from BMDM, primary HSC, and liver tissues was extracted using TRIzol reagents (Thermo Fisher Scientific), and reverse transcription of the RNA to cDNA with a reverse transcription kit (Promega) was performed in accordance with the manufacturer's guidelines. An SYBR Green Master mix was utilized to conduct qRT-PCR analysis. The $2^{-\Delta\Delta CT}$ method was employed to calculate the relative mRNA level. The primers for α-SMA, collagen type 1 alpha 1 (Col1A1), TGF-β, interleukin 4 (IL-4), MMP2, iNOS, TIMP1, MCP-1, LEF1, and c-Myc are shown in Table S1.

Western Blot Analysis. Proteins from BMDM, primary HSC, and liver tissues were isolated using a radioimmunoprecipitation assay extraction buffer. Subsequently, 10% sodium dodecyl sulfate polyacrylamide gel electrophoresis was utilized to separate the proteins, which were then transferred to a polyvinylidene difluoride (PVDF) membrane. Anti-α-SMA, antitype I collagen, anti-P-β-catenin, anti-c-Myc, anti-LEF1, anti-iNOS, anti-MCP-1, anti-TIMP1, anti-MMP2, anti-GPX4, anti-ACSL4, anti-SLC7A11, and anti-β-actin (an internal control) primary antibodies were applied to the PVDF membranes and incubated at 4 °C overnight followed by incubation with a secondary antibody for 1 h at ambient temperature.

Lipid ROS Assay. The lipid ROS level was measured as previously described.[20] In brief, BMDM was exposed to LPS for 24 h and then treated with or without Sch B (30 μM). Subsequently, the supernatant collected as the conditioned medium (CM) was used to culture primary HSCs treated with RAS-selective lethal 3 (RSL3, a potent inducer of FPT) and/or ferrostatin-1 (Fer-1, an inhibitor of FPT) for 24 h. At the end of the period, the culture medium was replaced by 1 mL of the BODIPY-C11 (Amgicam) dye for an additional 1 h. Cells were collected and subsequently washed twice with PBS before being resuspended in 500 μL of PBS. A 70 μm cell strainer was employed to filter the cell suspension, and then, the amount of ROS in cells was measured. A FACS Calibur Flow Cytometer (BD, USA) was used for analysis, and data were processed by using the FlowJo software.

RNA-Sequencing (RNA-seq) Profiling. BMDMs were stimulated with LPS (100 ng/mL) for 24 h and then treated with or without Sch B (30 μM) for 24 h in culture dishes. A Trizol reagent was used to collect the total RNA. After NanoDrop quality inspection and quantification, 1−2 μg of RNA was selected from each sample to construct the RNA-sequencing library. The total RNA sample was enriched by oligo dT (rRNA removal), and then, the library was constructed using a KAPA StrandedRNA-Seq Library Prep Kit (Illumina). The quality of the library was identified by an Agilent 2100 bioanalyzer. The sample libraries were sequenced with an Illumina NovaSeq6000 sequencer. Expressions of transcripts with Log_2 fold change$l > 2$, adjusted $P < 0.05$, were deemed statistically significant.

Isolation and Culture of Primary HSCs. Primary HSCs were isolated as in the previous study.[21] Primary HSCs were cultured in 35 mm dishes containing complete media consisting of DMEM with 10% FBS at a density of 4×10^5/mL. Cells were incubated at 37 °C in a humid environment with 5% CO_2, with media changes occurring every 2 days. Isolated primary HSCs were obtained through enzyme digestion and density gradient centrifugation, and the purity of the cells was greater than 98% through α-SMA and Desmin immunocytochemical staining.

Cell Culture. BMDM was treated with LPS (100 ng/mL) for 24 h and then treated with Sch B (30 μM) and Wnt agonist 1 (10 ng/mL). Subsequently, the supernatant was used as the CM to culture primary HSC. Primary HSCs, isolated from C57BL/6J mice, were induced by the above CM and treated with RSL3 (1 μM) and/or Fer-1 (1 μM) for an additional 24 h.

Cell Viability Assay. Cell viability was assessed using a cell counting kit-8 (CCK-8) assay as per the manufacturer's instructions. Primary HSCs (7×10^3) were seeded in 96-well plates and then exposed to the indicated treatment. Subsequently, CCK-8 reagents (GLPBIO Biotechnology) were added to the culture medium for 3 h. The optical densities of the wells were then measured with a microplate reader at 450 nm.

Flow Cytometry (FCM) Analysis. Briefly, BMDMs were cultured at 4 °C for 20 min with fluorescein isothiocyanate (FITC)-labeled antimouse Ly6C and phycoerythrin (PE)-labeled antimouse F4/80 (4A Biotech Co., Ltd., China) antibodies before washing twice with PBS. A FACS Calibur Flow Cytometer (BD, USA) was used for analysis, and data were processed using the FlowJo software.

Transmission Electron Microscopy (TEM). Cells were first fixed in an electron microscope fixative for 2−4 h, embedded in 1% agarose, and then dehydrated. Thin sections (60−80 nm) were then cut by using an ultramicrotome (Leica UC7, Leica). Afterward, sections were treated with uranyl acetate in pure ethanol for 15 min and then stained with lead citrate for 15 min. Representative images were obtained using TEM (HT7700, HITACHI).

Iron Measurements. HSCs were homogenized at a rapid rate in an iron assay buffer as per the instructions of an iron assay kit (Sigma-Aldrich) as previously described.[20] This process entailed the addition of an acidic buffer to release iron, which was measured to determine the total iron concentration. Subsequently, the solution was centrifuged at 13,000*g* for 10 min to remove the insoluble material, and the iron concentration was then assessed at 593 nm with a microplate fluorometer.

Detection of Malondialdehyde (MDA) and Glutathione (GSH) Levels. The levels of MDA and GSH were evaluated using MDA and GSH activity assay kits, respectively, as per the manufacturer's instructions. MDA and GSH contents were measured at 450 and 405 nm, respectively, with the help of a microplate fluorometer.

Statistical Analysis. Data were expressed as the mean ± standard deviation (SD). Student's *t*-test was used to differentiate two groups, and the one-way analysis of variance was applied to compare multiple groups. Statistical analyses were conducted using SPSS version 23.0 (SPSS, Chicago, IL), with a significance level of $P < 0.05$.

RESULTS

Sch B Alleviates CCl_4-Mediated Liver Fibrosis *In Vivo*. Whether Sch B has an inhibitory effect on liver fibrosis was examined in a CCl_4-induced mouse model of liver fibrosis. Compared with the control, analysis of Masson staining and Sirius red staining revealed CCl_4-induced collagen deposition (Figure 1B−E). Results of Hyp additionally showed that CCl_4 resulted in collagen upregulation (Figure 1F). Moreover, there was a significant increase in ALT and AST in CCl_4-treated mice compared with those in the control mice (Figure 1G,H). Overall, our data confirmed the establishment of a CCl_4-

https://doi.org/10.1021/acs.jafc.3c03409
J. Agric. Food Chem. 2023, 71, 17295−17307

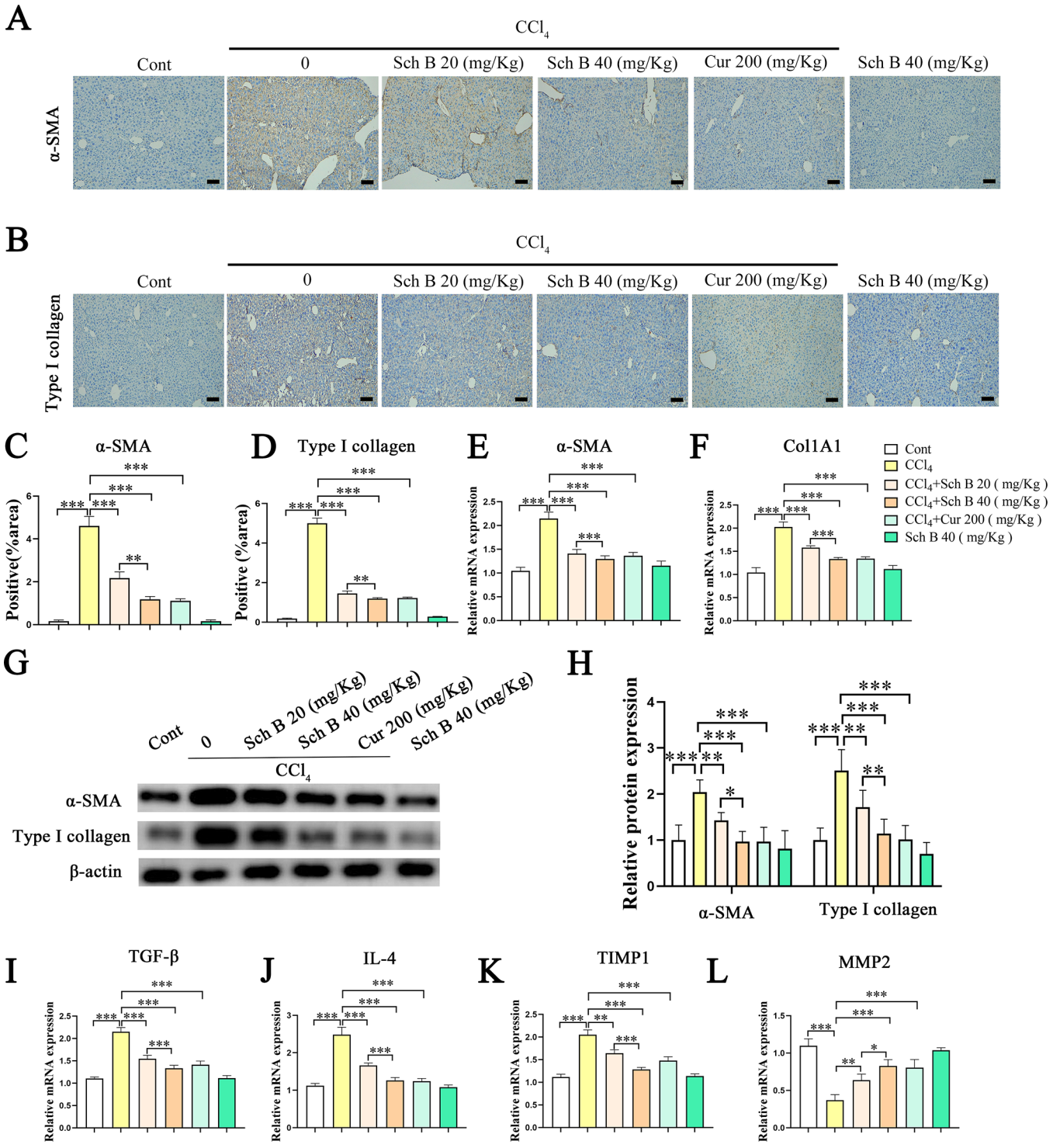

Figure 2. Sch B decreases the levels of α-SMA and Col1A1 and enhances antifibrotic factors in the liver. (A–D) Immunohistochemical staining analysis of α-SMA and type I collagen in the liver. Scale bars, 100 μm. (E, F) mRNA expressions of α-SMA and Col1A1 in the liver tissue. (G, H) Protein expressions of α-SMA and type I collagen in the liver tissue. (I–L) mRNA expressions of TGF-β, IL-4, TIMP1, and MMP2 in the liver tissue. Each value is the mean ± SD of six experiments. *P < 0.05, **P < 0.01, and ***P < 0.001.

treated mouse model. Notably, Sch B had a suppressive effect on CCl_4-induced collagen deposition (Figure 1B–F), suggesting the inhibitory effect of Sch B on liver fibrosis. Analysis of ALT and AST showed that the injured liver function in CCl_4-treated mice was restored by Sch B (Figure 1G,H). It was found that Sch B inhibited liver fibrosis in CCl_4-treated mice in a dose-dependent manner. Cur, an effective drug for treating liver fibrosis, was used as a positive control. Consistent with the results of Sch B, Cur contributed to the inhibition of the CCl_4-induced collagen level and liver function damage (Figure 1B–H). Interestingly, Sch B had no effect on healthy controls (Figure 1B–H). Together, our experiments illustrate that Sch B is effective in reducing CCl_4-mediated liver fibrosis *in vivo*.

https://doi.org/10.1021/acs.jafc.3c03409
J. Agric. Food Chem. 2023, 71, 17295–17307

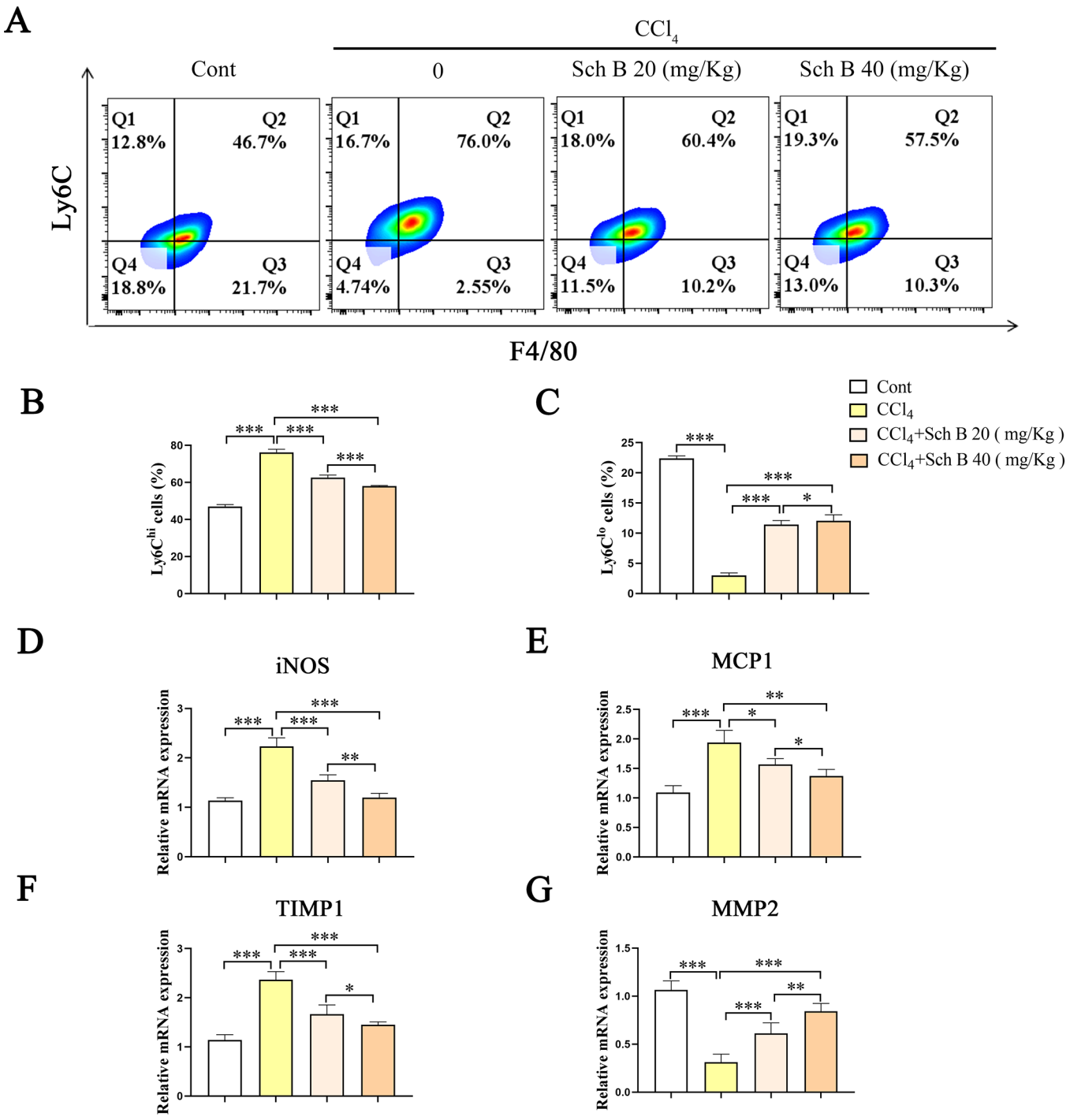

Figure 3. Sch B induces an increase in Ly6C^{lo} macrophages. (A−C) FCM analysis of the Ly6C level. (D−G) mRNA expressions of iNOS, MCP-1, TIMP1, and MMP2 *in vivo*. Each value is the mean ± SD of six experiments. *P < 0.05, **P < 0.01, and ***P < 0.001.

Further studies were performed to confirm the inhibitory role of Sch B *in vivo*. Analysis of α-SMA immunohistochemical staining indicated a reduction in the level of α-SMA protein in CCl_4-treated mice after Sch B treatment (Figure 2A,C). Moreover, the immunohistochemical results of reduced type I collagen by Sch B were found in CCl_4-treated mice (Figure 2B,D). In addition, Sch B induced a significant decrease in the mRNA and protein expressions of α-SMA and Col1A1 in CCl_4-treated mice in a dose-dependent manner (Figure 2E−H). It was found that pro-fibrotic factors including TGF-β, IL-4, and TIMP1 were reduced in liver tissues from the CCl_4 + Sch B group, whereas antifibrotic factor MMP2 was enhanced (Figure 2I−L). Similar results were also found in CCl_4-treated mice after Cur treatment (Figure 2A−L). Our data suggest that Sch B could inhibit liver fibrosis, at least in part, via suppressing pro-fibrotic factors and enhancing antifibrotic factors.

Sch B Induces an Increase in Ly6C^{lo} Macrophages. Macrophages have been reported to secrete pro-fibrotic factors as well as antifibrotic factors in the involvement of HSC activation.[22] It is known that Ly6C^{hi} macrophages are the predominant macrophage type in the injured liver and are

https://doi.org/10.1021/acs.jafc.3c03409
J. Agric. Food Chem. 2023, 71, 17295−17307

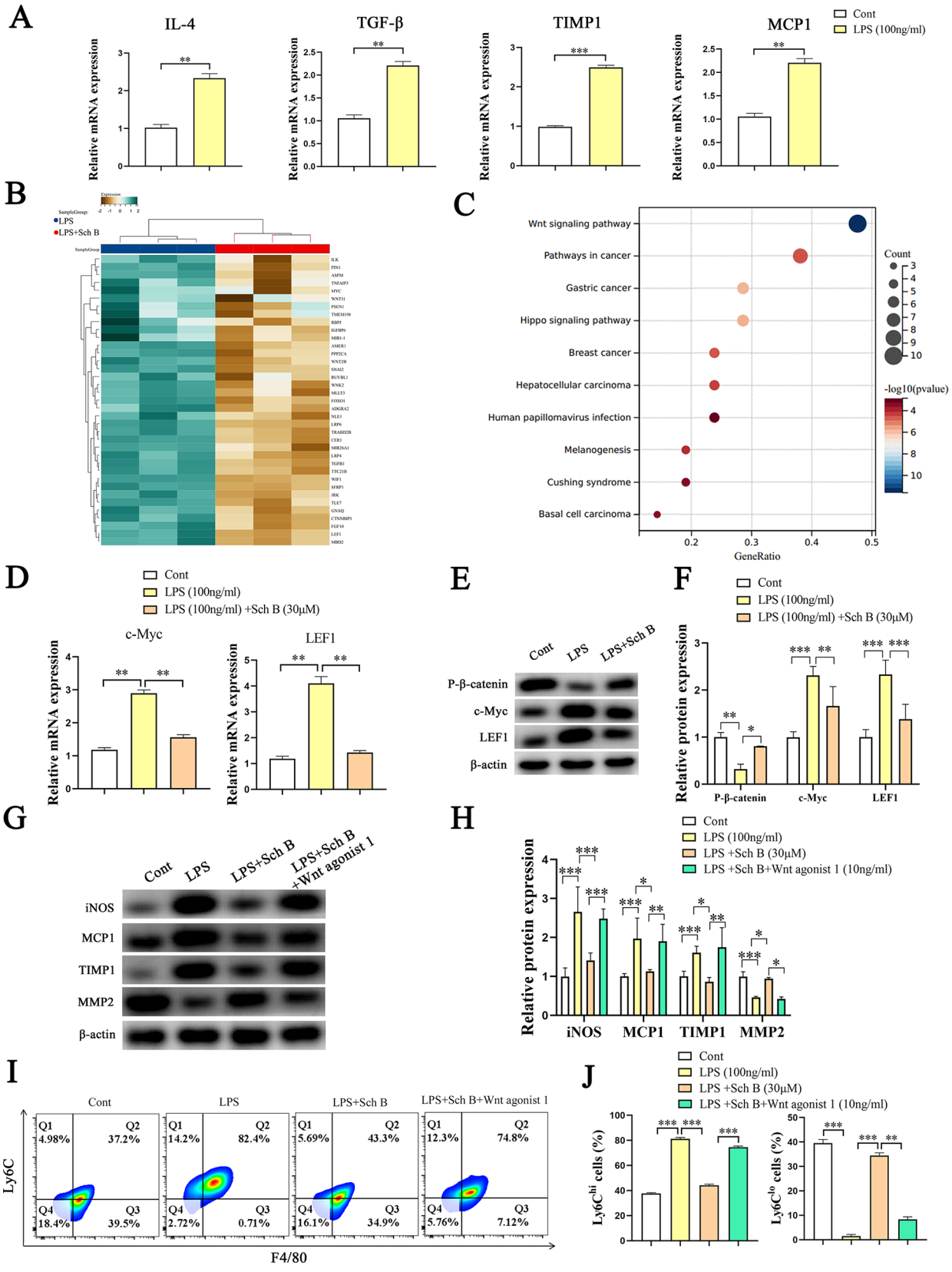

Figure 4. Sch B upregulates the expression of Ly6C^{lo} macrophages via Wnt/β-catenin pathway BMDMs, isolated from control group mice, that were treated with LPS (100 ng/mL) for 24 h and then treated with Sch B (30 μM) for an additional 24 h. (A) mRNA expressions of IL-4, TGF-β, TIMP1, and MCP-1 in BMDMs. (B, C) KEGG analysis and heatmap. (D) mRNA expressions of c-Myc and LEF1. (E, F) Protein expressions of P-β-catenin, c-Myc, and LEF1. (G, H) Proteins expressions of iNOS, MCP-1, TIMP1, and MMP2. (I, J) Expression of Ly6C was detected by FCM. Each value is the mean ± SD of three experiments. *P < 0.05, **P < 0.01, and ***P < 0.001.

https://doi.org/10.1021/acs.jafc.3c03409
J. Agric. Food Chem. 2023, 71, 17295−17307

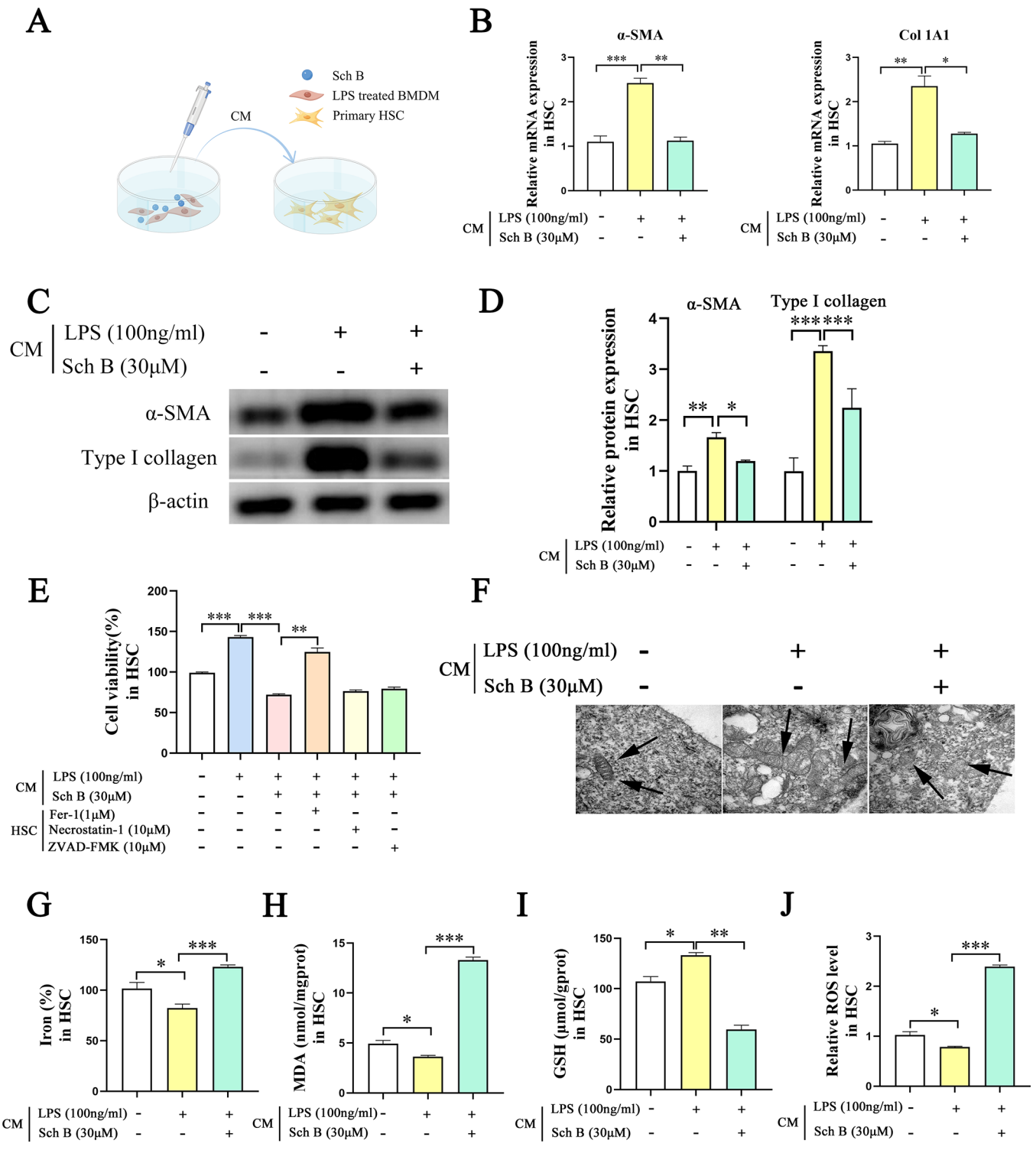

Figure 5. Sch B-mediated Ly6C^{lo} macrophages promote HSC FPT BMDMs that were treated with LPS (100 ng/mL) for 24 h and then treated with Sch B (30 μM) for an additional 24 h. Subsequently, the supernatant was used as the CM to coculture with primary HSCs. (A) Illustration of the generation of CM. (B) mRNA expressions of α-SMA and Col1A1 in primary HSCs. (C, D) Protein expressions of α-SMA and type I collagen in primary HSCs. (E) Cell viability. (F) TEM analysis. Scale bar, 0.2 μm. (G–J) Levels of iron, MDA, GSH, and ROS in primary HSCs. Each value is the mean ± SD of three experiments. *P < 0.05, **P < 0.01, and ***P < 0.001.

essential for HSC activation. Therefore, whether Sch B has an effect on macrophage phenotypic transformation was next explored in BMDMs after Sch B treatment. FCM analysis showed that compared with CCl_4-treated mice, Sch B caused a reduction in the number of Ly6C^{hi} macrophages and an increase in the number of Ly6C^{lo} macrophages (Figure 3A–C). Consistent with this, iNOS (a pro-inflammation factor) and MCP-1 (a pro-fibrotic factor) were downregulated in CCl_4 + Sch B groups (Figure 3D,E). In addition, in comparison with the CCl_4 group, increased MMP2 and reduced TIMP1 were found in BMDMs from CCl_4 mice treated with Sch B (Figure 3F,G). Collectively, these findings suggest that the Ly6C^{lo}

https://doi.org/10.1021/acs.jafc.3c03409
J. Agric. Food Chem. 2023, 71, 17295−17307

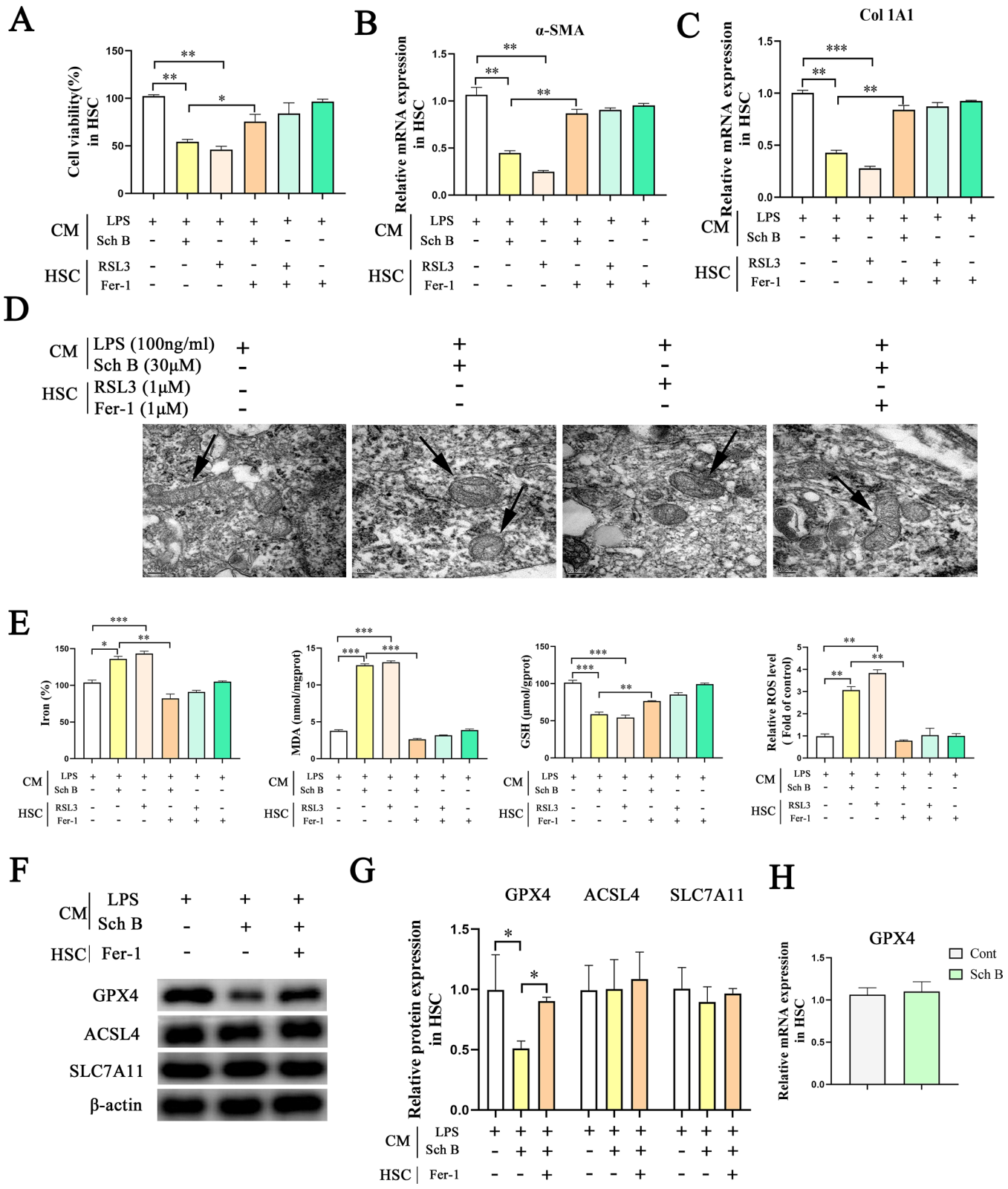

Figure 6. Sch B-treated BMDMs promote HSC FPT via GPX4 BMDMs that were treated with LPS (100 ng/mL) for 24 h and additionally treated with Sch B (30 μM) for 24 h; then, the resulting supernatant was used as the CM. Primary HSCs with RSL3 (1 μM) and Fer-1 (1 μM) were cocultured with the CM. (A) Cell viability. (B, C) mRNA expressions of α-SMA and Col1A1 in primary HSCs. (D) TEM analysis. Scale bar, 0.2 μm. (E) Levels of iron, MDA, GSH, and ROS in primary HSCs. (F, G) Protein expressions of GPX4, ACSL4, and SLC7A11. (H) mRNA expression of GPX4. Each value is the mean ± SD of three experiments. *P < 0.05, **P < 0.01, and ***P < 0.001.

macrophage transformation is involved in the inhibitory roles of Sch B in liver fibrosis and inflammation.

Sch B Upregulates the Number of Ly6C^{lo} Macrophages via the Wnt/β-Catenin Pathway. Next, LPS was

https://doi.org/10.1021/acs.jafc.3c03409
J. Agric. Food Chem. 2023, 71, 17295−17307

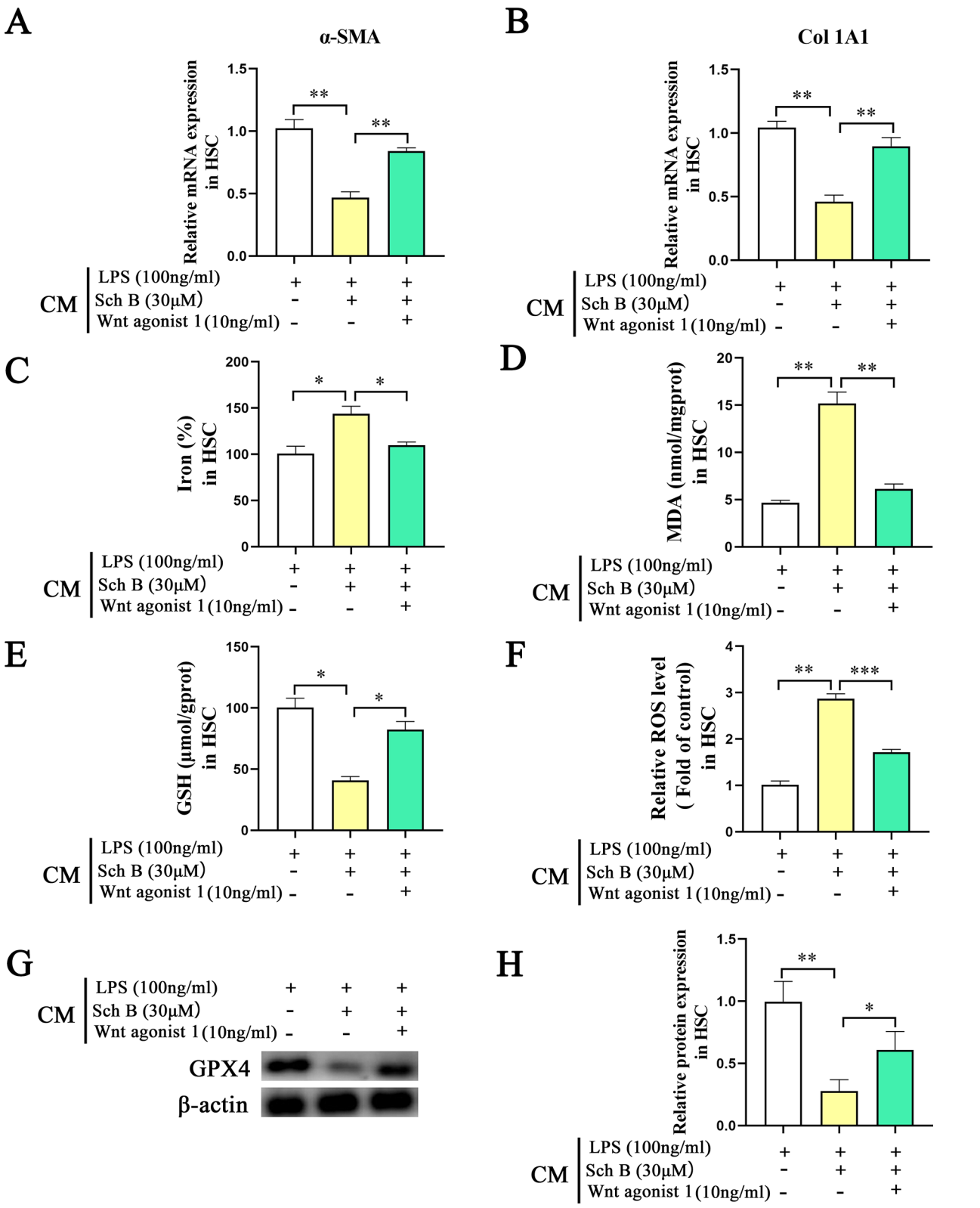

Figure 7. Sch B-treated BMDM-mediated HSC FPT is associated with Wnt/β-catenin pathway activation BMDMs that were treated with LPS (100 ng/mL) for 24 h and then treated with Sch B (30 μM) and Wnt agonist 1 (10 ng/mL) for an additional 24 h. Then, primary HSCs were cocultured with the above CM. (A, B) mRNA expressions of α-SMA and Col1A1 in primary HSCs. (C−F) Levels of iron, MDA, GSH, and ROS in primary HSCs. (G, H) Protein expressions of GPX4 in primary HSCs. Each value is the mean ± SD of three experiments. *P < 0.05, **P < 0.01, and ***P < 0.001.

used to induce BMDM activation. Clearly, LPS significantly elevated the expression levels of IL-4, TGF-β, TIMP1, and MCP-1 in BMDMs compared to the control (Figure 4A), indicating that LPS successfully induces inflammation. Then,

https://doi.org/10.1021/acs.jafc.3c03409
J. Agric. Food Chem. 2023, 71, 17295−17307

to explore the potential mechanism for the Sch B-mediated Ly6C^{lo} macrophage transformation, LPS-activated BMDMs were treated with Sch B. RNA-seq was conducted to determine the potential pathways involved in the effects of Sch B on the Ly6C^{lo} transformation (Figure 4B). KEGG analysis of the differentially expressed genes revealed that the Wnt pathway was highly involved in the effects of Sch B on Ly6C^{lo} macrophage transformation (Figure 4B,C). Therefore, the Wnt pathway was selected for the subsequent experiments.

The Wnt/β-catenin signaling pathway has been demonstrated to play an important role in HSC activation and liver fibrosis development.[23] Next, the expressions of P-β-catenin and Wnt pathway-related genes such as LEF1 and c-Myc were examined in LPS-treated BMDMs after Sch B treatment. Our results showed that LPS caused an increase in c-Myc and LEF1 and a reduction in P-β-catenin, which was blocked down by Sch B (Figure 4D−F). To further confirm that Sch B-mediated Ly6C macrophage phenotypic transformation is via Wnt/β-catenin signaling, Sch B-treated BMDMs were additionally treated with Wnt agonist 1 (Wnt/β-catenin pathway activator). The results of western blots showed that Sch B effectively inhibited LPS-mediated upregulation of iNOS, MCP-1, and TIMP1 as well as downregulation of MMP2, which was reversed by Wnt agonist 1 (Figure 4G,H). Data from FCM analysis also demonstrated that increased Ly6C^{lo} was suppressed by Wnt agonist 1 in BMDMs (Figure 4I,J). Collectively, these findings suggest that Sch B-mediated Ly6C macrophage phenotype transformation is via the Wnt/β-catenin pathway.

Sch B-Mediated Ly6C^{lo} Macrophages Promote HSC FPT. Whether Sch B-mediated Ly6C^{lo} macrophages contribute to HSC inactivation was further explored. Primary HSCs were cocultured with the CM from LPS and Sch B-treated BMDMs (Figure 5A), and the levels of HSC activation-related genes including α-SMA and Col1A1 were examined. Compared with the control, CM from LPS-treated BMDMs led to increased levels of α-SMA and Col1A1 (Figure 5B−D). Interestingly, reduced mRNA and protein levels of α-SMA and Col1A1 were found in HSCs cocultured with CM from LPS-treated BMDMs after Sch B treatment (Figure 5B−D). Combined with these, we demonstrate that Sch B-mediated Ly6C^{lo} macrophages could suppress HSC activation.

Next, we explored whether Sch B-mediated Ly6C^{lo} macrophages promote HSC FPT. It was found that CM from Sch B-treated BMDMs effectively induced cell death in HSCs, which was inhibited by an FPT inhibitor, Fer-1. However, ZVAD-FMK (an apoptotic inhibitor) and Necrostatin-1 (a necroptosis inhibitor) had no effect on Sch B-caused cell death (Figure 5E). Together, we demonstrate that Sch B-induced cell death is associated with FPT, not apoptosis or necrosis. TEM analysis further showed that CM from Sch B-treated BMDMs promoted the disappearance of HSC mitochondrial cristae and the rupture of the outer membrane (Figure 5F). Generally, FPT is dependent on intracellular iron and characterized by lipid peroxidation. Clearly, CM from Sch B-treated BMDMs led to reduced GSH as well as increased ROS, iron, and MDA (Figure 5G−J). Taken together, all of these results indicate that Sch B-mediated Ly6C^{lo} macrophages may promote HSC FPT.

Sch B-Treated BMDMs Promote HSC FPT via GPX4. Further studies were performed to determine the underlying mechanism of Sch B-mediated HSC FPT. Then, primary HSCs with RSL3 (an FPT inducer) or Fer-1 (an FPT inhibitor) were cocultured with BMDMs after Sch B treatment. Obviously, compared with the LPS group, CM from Sch B-treated BMDMs induced HSC death, which was in line with the results of RSL3 (Figure 6A). Notably, the effect of CM from Sch B-treated BMDMs on HSC death was inhibited by Fer-1 (Figure 6A). Similarly, CM from Sch B-treated BMDMs (or RSL3) decreased HSC activation, including reduced α-SMA and Col1A1, which could be inhibited by Fer-1 (Figure 6B,C). Results from TEM confirmed that CM from Sch B-treated BMDMs (or RSL3) promoted the disappearance of HSC mitochondrial cristae, which was blocked by Fer-1 (Figure 6D). Finally, both CM from Sch B-treated BMDMs and RSL3 contributed to HSC FPT, resulting in reduced GSH as well as enhanced ROS, iron, and MDA (Figure 6E). Moreover, the effects of CM from Sch B-treated BMDMs on HSC FPT were suppressed by Fer-1 (Figure 6E). Our results suggest that Sch B-treated BMDMs could promote HSC FPT.

Recently, several FPT-associated genes such as GPX4, ACSL4, and SLC7A11 have been reported to participate in the FPT process.[24] Next, GPX4, ACSL4, and SLC7A11 were examined in HSCs cocultured with CM from Sch B-treated BMDMs. Our results indicated that reduced GPX4 (a negative regulator of FPT) was found in HSCs cocultured with CM from Sch B-treated BMDMs, whereas ACSL4 and SLC7A11 were not found (Figure 6F,G). Notably, Sch B had no direct regulatory effect on GPX4 in primary HSCs (Figure 6H), indicating that Sch B-treated BMDMs promote HSC FPT, at least in part, via GPX4 from CM. In line with this, the inhibitory effect of CM from Sch B-treated BMDMs on GPX4 was inhibited by Fer-1 (Figure 6F,G), suggesting that Fer-1-inhibited HSC FPT is also associated with GPX4. Combined with these, our data suggest that Sch B-treated BMDMs induce HSC FPT, at least in part, via GPX4 from CM.

Sch B-Treated BMDM-Mediated HSC FPT Is Associated with Wnt/β-Catenin Pathway Activation. Last, further studies were performed to confirm the role of the Wnt/β-catenin pathway in BMDM-mediated HSC FPT. Then, the levels of α-SMA and Col1A1 in HSCs cocultured with CM from Sch B-treated BMDMs after Wnt agonist 1 treatment were examined. In HSCs cocultured with CM from Sch B-treated BMDMs, reduced α-SMA and Col1A1 were restored by Wnt agonist 1 (Figure 7A and Figure 7B, respectively). Moreover, the FPT process in HSCs cocultured with CM from Sch B-treated BMDMs was blocked down by Wnt agonist 1, with increased GSH as well as reduced iron level, MDA, and ROS (Figure 7C−F). In addition, reduced GPX4 in HSCs cocultured with CM from Sch B-treated BMDMs was reversed by Wnt agonist 1 (Figure 7G,H). Taken together, all of these data suggest that Sch B-inhibited Wnt pathway activation contributes to increased Ly6C^{lo}, which finally leads to HSC FPT.

DISCUSSION

It is well known that activated HSCs contribute to the development of liver fibrosis. Upon injury, HSCs differentiate into activated myofibroblasts, secreting and accumulating fibrillar collagen, leading to extensive fibrosis. Therefore, suppressing activation of HSC is an effective approach for treating liver fibrosis.[25] Sch B has been reported to have antioxidant, anti-inflammatory, anti-immunological, and cardiac protective effects. For example, Sch B synergizes docetaxel-induced restriction of growth and invasion of cervical cancer cells.[26] Chen et al. found that Sch B attenuates liver

https://doi.org/10.1021/acs.jafc.3c03409
J. Agric. Food Chem. 2023, 71, 17295−17307

fibrosis by regulation of Nrf2-ARE and TGF-β/Smad signaling pathways.[27] In this study, Sch B had an inhibitory role in liver fibrosis *in vivo* and *in vitro*. Owing to the Wnt/β-catenin pathway inactivation, Sch B upregulated the number of Ly6C^{lo} macrophages, leading to HSC FPT and inactivation. We demonstrate the involvement of the Wnt/β-catenin pathway in Ly6C^{lo} macrophage transformation and HSC FPT, and this is the first report.

It is known that macrophages undergo marked phenotypic and functional changes to fulfill essential functions during the initiation, maintenance, and resolution phases of tissue repair.[28] Increasing evidence has demonstrated that Ly6C^{hi} macrophages are responsible for initiating fibrosis, while Ly6C^{lo} macrophages participate in the inhibition of fibrosis development. For example, Bhatia et al. revealed that Ly6C^{hi} promotes kidney fibrosis in mice via the PINK1/MFN2/Parkin-mediated pathway.[29] Li et al. reported that suppressing the infiltration of Ly6C^{hi} monocytes can alleviate liver fibrosis.[30] Combined with these, inhibiting Ly6C^{hi} macrophage phenotypic transformation or increasing the Ly6C^{lo} number may be a promising approach for treating liver fibrosis. Herein, it was found that Sch B could upregulate the number of Ly6C^{lo}. Sch B-induced Ly6C^{lo} was found to promote HSC FPT and resulted in increased MMP2 as well as reduced TIMP1, which finally inhibited liver fibrosis.

Wnt signaling, an evolutionarily conserved pathway, is crucial for embryonic development and tissue homeostasis. The Wnt/β-catenin pathway, canonical signaling of Wnt, has been reported to be associated with the development of cancers and fibrosis, such as HCC and liver fibrosis. Recent studies have shown the involvement of the Wnt/β-catenin pathway in the regulation of macrophage function. Yang et al. found that tumor cell-derived Wnt ligands promote M2-like macrophage polarization via canonical Wnt/β-catenin signaling, thus facilitating tumor growth and migration in HCC.[31] Lai et al. reported that the abnormal activated Wnt signaling pathway is crucial for liver fibrosis progression.[32] In this study, results of RNA-seq and KEGG pathway enrichment analysis collectively indicated that the Wnt/β-catenin signaling pathway may be responsible for the effect of Sch B on the phenotypic transformation of Ly6C^{lo}. Further studies revealed that Sch B enhanced P-β-catenin (a negative regulator for Wnt/β-catenin signaling) and suppressed LEF1 and c-Myc (key components of Wnt/β-catenin signaling). In addition, restoration of Wnt/β-catenin pathway activation inhibited Sch B-mediated Ly6C^{lo} transformation and HSC FPT. Combined with these, our data revealed the importance of Wnt/β-catenin pathway activation in the transformation of Ly6C^{lo} macrophage phenotypic transformation. Moreover, Sch B-inhibited Wnt pathway activation contributed to an increased Ly6C^{lo}, which finally led to HSC FPT.

FPT, an iron-dependent nonapoptotic cell death, has been reported to participate in cancer development such as HCC.[33] Increasing evidence has shown the potential benefits that FPT may offer in terms of liver fibrosis treatment and prevention.[34] However, the underlying mechanisms of HSC FPT are still largely unknown. Herein, we found that CM from Sch B-treated BMDMs contributed to HSC FPT, especially for mitochondrial cristae deletion. It was found that GPX4, a negative regulator of FPT, was reduced in HSCs cocultured with the CM from Sch B-treated BMDMs. In addition, Sch B had no direct regulatory effect on GPX4 in primary HSCs. Interestingly, the effects of CM from Sch B-treated BMDMs on HSC FPT were suppressed by Fer-1. Notably, the inhibitory effect of CM from Sch B-treated BMDMs on GPX4 was inhibited by Fer-1. Combined with these, our results suggest that the crosstalk between macrophage and HSC FPT may be, at least in part, via GPX4.

In conclusion, we demonstrate that Sch B inhibits Wnt pathway activation and induces an increase in Ly6C^{lo} macrophages, which finally contributes to HSC FPT. Sch B may be a promising drug for liver fibrosis treatment.

■ ASSOCIATED CONTENT

Supporting Information

The Supporting Information is available free of charge at https://pubs.acs.org/doi/10.1021/acs.jafc.3c03409.

Primers used for qRT-PCR (Table S1) (PDF)

■ AUTHOR INFORMATION

Corresponding Author

Jianjian Zheng − *Key Laboratory of Clinical Laboratory Diagnosis and Translational Research of Zhejiang Province, The First Affiliated Hospital of Wenzhou Medical University, Wenzhou 325000, China;* orcid.org/0000-0001-8770-4219; Email: zjj@wmu.edu.cn

Authors

Xinmiao Li − *Key Laboratory of Diagnosis and Treatment of Severe Hepato-Pancreatic Diseases of Zhejiang Province, The First Affiliated Hospital of Wenzhou Medical University, Wenzhou 325000, China*

Feng Jiang − *Key Laboratory of Clinical Laboratory Diagnosis and Translational Research of Zhejiang Province, The First Affiliated Hospital of Wenzhou Medical University, Wenzhou 325000, China*

Yuhang Hu − *Key Laboratory of Diagnosis and Treatment of Severe Hepato-Pancreatic Diseases of Zhejiang Province, The First Affiliated Hospital of Wenzhou Medical University, Wenzhou 325000, China*

Zhichao Lang − *Key Laboratory of Diagnosis and Treatment of Severe Hepato-Pancreatic Diseases of Zhejiang Province, The First Affiliated Hospital of Wenzhou Medical University, Wenzhou 325000, China*

Yating Zhan − *Key Laboratory of Diagnosis and Treatment of Severe Hepato-Pancreatic Diseases of Zhejiang Province, The First Affiliated Hospital of Wenzhou Medical University, Wenzhou 325000, China*

Rongrong Zhang − *Key Laboratory of Diagnosis and Treatment of Severe Hepato-Pancreatic Diseases of Zhejiang Province, The First Affiliated Hospital of Wenzhou Medical University, Wenzhou 325000, China*

Qiqi Tao − *Key Laboratory of Diagnosis and Treatment of Severe Hepato-Pancreatic Diseases of Zhejiang Province, The First Affiliated Hospital of Wenzhou Medical University, Wenzhou 325000, China*

Chengchu Luo − *Key Laboratory of Diagnosis and Treatment of Severe Hepato-Pancreatic Diseases of Zhejiang Province, The First Affiliated Hospital of Wenzhou Medical University, Wenzhou 325000, China*

Jinglu Yu − *Key Laboratory of Diagnosis and Treatment of Severe Hepato-Pancreatic Diseases of Zhejiang Province, The First Affiliated Hospital of Wenzhou Medical University, Wenzhou 325000, China; Department of Laboratory*

Medicine, Lishui Municipal Central Hospital, Lishui 323020, China

Complete contact information is available at: https://pubs.acs.org/10.1021/acs.jafc.3c03409

Author Contributions

J.Z. designed the study. X.L., F.J., Y.H., R.Z., and Z.L. performed most of the experiments. Q.T. and C.L. analyzed the data and wrote the manuscript. Y.Z. and J.Y. revised and offered advice about the manuscripts. All authors contributed to the article and approved the submitted version.

Funding

The project was supported by the Wenzhou Municipal Science and Technology Bureau (no. Y20220023), Key Laboratory of Clinical Laboratory Diagnosis and Translational Research of Zhejiang Province (no. 2022E10022), the project of Wenzhou Medical University Basic Scientific Research (no. KYYW201904), and Key Laboratory of Diagnosis and Treatment of Severe Hepatopancreatic Diseases of Zhejiang Province (grant no. 2018E10008).

Notes

The authors declare no competing financial interest.

All the animal procedures were approved by the Laboratory Animal Ethics Committee of Wenzhou Medical University (no. wydw2022−0757).

■ ACKNOWLEDGMENTS

Figure 5A and TOC Figure were drawn by Figdraw (ID: AIWUA37665 and SPAOPe7644).

■ ABBREVIATIONS

Sch B, Schisandrin B; HSC, hepatic stellate cell; CCl_4, carbon tetrachloride; Ly6C, lymphocyte antigen 6 complex locus C; Hyp, hydroxyproline; ALT, alanine aminotransferase; AST, aspartate aminotransferase; α-SMA, alpha-smooth muscle actin; qRT-PCR, quantitative real-time polymerase chain reaction; Col1A1, collagen type 1 alpha 1; LPS, lipopolysaccharide; CCK-8, cell counting kit-8; TGF-β, transforming growth factor β; IL-4, interleukin 4; TIMP1, tissue inhibitor of metalloproteinases 1; MMP2, matrix metalloproteinase 2; iNOS, inducible nitric oxide synthase; MCP-1, monocyte chemoattractant protein-1; LEF1, lymphoid enhancement factor 1; BMDM, bone marrow-deprived macrophage; RSL3, RAS-selective lethal 3; GSH, glutathione; MDA, malondialdehyde; ROS, reactive oxygen species; Fer-1, ferrostatin-1

■ REFERENCES

(1) Zhou, C.; York, S.; Chen, J.; Pondick, J.; Motola, D.; Chung, R.; Mullen, A. Long noncoding RNAs expressed in human hepatic stellate cells form networks with extracellular matrix proteins. *Genome Med.* **2016**, *8* (1), 31.

(2) Liu, S.; Han, D.; Xu, C.; Yang, F.; Li, Y.; Zhang, K.; Zhao, X.; Zhang, J.; Lu, T.; Lu, S.; Shi, C.; Zhang, R.; Yang, A.; Zhao, A.; Qin, W.; Yang, B.; Wen, W. Antibody-drug conjugates targeting CD248 inhibits liver fibrosis through specific killing on myofibroblasts. *Mol. Med.* **2022**, *28* (1), 37.

(3) Wynn, T. A.; Vannella, K. M. Macrophages in Tissue Repair, Regeneration, and Fibrosis. *Immunity* **2016**, *44* (3), 450−462.

(4) Duan, M.; Yang, Y.; Peng, S.; Liu, X.; Zhong, J.; Guo, Y.; Lu, M.; Nie, H.; Ren, B.; Zhang, X.; Liu, L. Schistosoma japonicum C/EBP Homologous Protein (CHOP) Activates Macrophages and Promotes Liver Fibrosis in -Infected Mice. *J. Immunol. Res.* **2019**, *2019*, 5148575.

(5) Jäppinen, N.; Félix, I.; Lokka, E.; Tyystjärvi, S.; Pynttäri, A.; Lahtela, T.; Gerke, H.; Elima, K.; Rantakari, P.; Salmi, M. Fetal-derived macrophages dominate in adult mammary glands. *Nat. Commun.* **2019**, *10* (1), 281.

(6) Tacke, F.; Zimmermann, H. W. Macrophage heterogeneity in liver injury and fibrosis. *J. Hepatol.* **2014**, *60* (5), 1090−6.

(7) Lan, T.; Li, C.; Yang, G.; Sun, Y.; Zhuang, L.; Ou, Y.; Li, H.; Wang, G.; Kisseleva, T.; Brenner, D.; Guo, J. Sphingosine kinase 1 promotes liver fibrosis by preventing mi R-19b-3p-mediated inhibition of CCR2. *Hepatology (Baltimore, Md.)* **2018**, *68* (3), 1070−1086.

(8) Iwakiri, Y. Nitric oxide in liver fibrosis: The role of inducible nitric oxide synthase. *Clin Mol. Hepatol* **2015**, *21* (4), 319−25.

(9) Du, Q.; Luo, J.; Yang, M.; Liu, Q.; Heres, C.; Yan, Y.; Stolz, D.; Geller, D. iNOS/NO is required for IRF1 activation in response to liver ischemia-reperfusion in mice. *Mol. Med.* **2020**, *26* (1), 56.

(10) Hamada, T.; Duarte, S.; Tsuchihashi, S.; Busuttil, R.; Coito, A. Inducible nitric oxide synthase deficiency impairs matrix metalloproteinase-9 activity and disrupts leukocyte migration in hepatic ischemia/reperfusion injury. *American journal of pathology* **2009**, *174* (6), 2265−77.

(11) Dixon, S.; Lemberg, K.; Lamprecht, M.; Skouta, R.; Zaitsev, E.; Gleason, C.; Patel, D.; Bauer, A.; Cantley, A.; Yang, W.; Morrison, B.; Stockwell, B. ferroptosis: an iron-dependent form of nonapoptotic cell death. *Cell* **2012**, *149* (5), 1060−72.

(12) Balihodzic, A.; Prinz, F.; Dengler, M.; Calin, G.; Jost, P.; Pichler, M. Non-coding RNAs and ferroptosis: potential implications for cancer therapy. *Cell death and differentiation* **2022**, *29* (6), 1094−1106.

(13) Gao, R.; Kalathur, R.; Coto-Llerena, M.; Ercan, C.; Buechel, D.; Shuang, S.; Piscuoglio, S.; Dill, M.; Camargo, F.; Christofori, G.; Tang, F. YAP/TAZ and ATF4 drive resistance to Sorafenib in hepatocellular carcinoma by preventing ferroptosis. *EMBO Mol. Med.* **2021**, *13* (12), No. e14351.

(14) Zhang, Z.; Guo, M.; Shen, M.; Kong, D.; Zhang, F.; Shao, J.; Tan, S.; Wang, S.; Chen, A.; Cao, P.; Zheng, S. The BRD7-P 53-SLC25A28 axis regulates ferroptosis in hepatic stellate cells. *Redox Biol.* **2020**, *36*, No. 101619.

(15) Yan, L.; Zhang, S.; Luo, G.; Cheng, B.; Zhang, C.; Wang, Y.; Qiu, X.; Zhou, X.; Wang, Q.; Song, X.; Pan, S.; Zhang, Y. Schisandrin B mitigates hepatic steatosis and promotes fatty acid oxidation by inducing autophagy through AMPK/mTOR signaling pathway. *Metabolism: clinical and experimental* **2022**, *131*, No. 155200.

(16) Zhang, H.; Chen, Q.; Dahan, A.; Xue, J.; Wei, L.; Tan, W.; Zhang, G. Transcriptomic analyses reveal the molecular mechanisms of schisandrin B alleviates CCl-induced liver fibrosis in rats by RNA-sequencing. *Chemico-biological interactions* **2019**, *309*, 108675.

(17) Lam, H.; Liang, T.; Peng, S. Ameliorative effects of Schisandrin B on Schistosoma mansoni-induced hepatic fibrosis in vivo. *PLoS neglected tropical diseases* **2021**, *15* (6), No. e0009554.

(18) Li, Y.; Zhang, T.; Liu, Q.; Zhang, J.; Li, R.; Pu, S.; Wu, T.; Ma, L.; He, J. Mixed micelles loaded with the 5-benzylidenethiazolidine-2, 4-dione derivative SKLB023 for efficient treatment of non-alcoholic steatohepatitis. *International journal of nanomedicine* **2019**, *14*, 3943−3953.

(19) Zhang, L.; Pavicic, P.; Datta, S.; Song, Q.; Xu, X.; Wei, W.; Su, F.; Rayman, P.; Zhao, C.; Hamilton, T. Unfolded Protein Response Differentially Regulates TLR4-Induced Cytokine Expression in Distinct Macrophage Populations. *Front. Immunol.* **2019**, *10*, 1390.

(20) Wang, Y.; Quan, F.; Cao, Q.; Lin, Y.; Yue, C.; Bi, R.; Cui, X.; Yang, H.; Yang, Y.; Birnbaumer, L.; Li, X.; Gao, X. Quercetin alleviates acute kidney injury by inhibiting ferroptosis. *Journal of advanced research* **2021**, *28*, 231−243.

(21) Kim, Y.; Ko, B.; Kim, D.; Tak, J.; Han, C.; Cho, J.; Kim, W.; Kim, S. Induction of the hepatic aryl hydrocarbon receptor by alcohol dysregulates autophagy and phospholipid metabolism via PPP2R2D. *Nat. Commun.* **2022**, *13* (1), 6080.

(22) Liu, L.; Wang, P.; Wang, Y.; Zhang, Y.; Li, C.; Yang, Z.; Liu, Z.; Zhan, T.; Xu, J.; Xia, C. MiR-130a-3p Alleviates Liver Fibrosis by Suppressing HSCs Activation and Skewing Macrophage to Ly6C Phenotype. *Frontiers in immunology* **2021**, *12*, No. 696069.
(23) Nishikawa, K.; Osawa, Y.; Kimura, K. Wnt/β-Catenin Signaling as a Potential Target for the Treatment of Liver Cirrhosis Using antifibrotic Drugs. *Int. J. Mol. Sci.* **2018**, *19* (10), 3103 DOI: 10.3390/ijms19103103.
(24) Wang, T.; Liang, J.; Zhang, C.; Xiong, Y.; Guan, K.; Yuan, H. The oncometabolite 2-hydroxyglutarate produced by mutant IDH1 sensitizes cells to ferroptosis. *Cell Death Dis.* **2019**, *10* (10), 755.
(25) Wang, F.; Jia, Y.; Li, M.; Wang, L.; Shao, J.; Guo, Q.; Tan, S.; Ding, H.; Chen, A.; Zhang, F.; Zheng, S. Blockade of glycolysis-dependent contraction by oroxylin a via inhibition of lactate dehydrogenase-a in hepatic stellate cells. *Cell Commun. Signaling* **2019**, *17* (1), 11.
(26) Yan, C.; Gao, L.; Qiu, X.; Deng, C. in vitro Schisandrin B synergizes docetaxel-induced restriction of growth and invasion of cervical cancer cells and. *Annals of translational medicine* **2020**, *8* (18), 1157.
(27) Chen, Q.; Zhang, H.; Cao, Y.; Li, Y.; Sun, S.; Zhang, J.; Zhang, G. Schisandrin B attenuates CCl (4)-induced liver fibrosis in rats by regulation of Nrf 2-ARE and TGF-β/Smad signaling pathways. *Drug Des Devel Ther* **2017**, *11*, 2179−2191.
(28) Wynn, T.; Vannella, K. Macrophages in Tissue Repair, Regeneration, and Fibrosis. *Immunity* **2016**, *44* (3), 450−462.
(29) Bhatia, D.; Chung, K.; Nakahira, K.; Patino, E.; Rice, M.; Torres, L.; Muthukumar, T.; Choi, A.; Akchurin, O.; Choi, M. Mitophagy-dependent macrophage reprogramming protects against kidney fibrosis. *JCI insight* **2019**, *4* (23), No. e132826, DOI: 10.1172/jci.insight.132826.
(30) Li, S.; Zhou, B.; Xue, M.; Zhu, J.; Tong, G.; Fan, J.; Zhu, K.; Hu, Z.; Chen, R.; Dong, Y.; Chen, Y.; Lee, K.; Li, X.; Jin, L.; Cong, W. Macrophage-specific FGF12 promotes liver fibrosis progression in mice. *Hepatology (Baltimore, Md.)* **2023**, *77* (3), 816−833.
(31) Yang, Y.; Ye, Y.; Chen, Y.; Zhao, J.; Gao, C.; Han, H.; Liu, W.; Qin, H. Crosstalk between hepatic tumor cells and macrophages via Wnt/β-catenin signaling promotes M2-like macrophage polarization and reinforces tumor malignant behaviors. *Cell Death Dis.* **2018**, *9* (8), 793.
(32) Lai, K. K. Y.; Kweon, S. M.; Chi, F.; Hwang, E.; Kabe, Y.; Higashiyama, R.; Qin, L.; Yan, R.; Wu, R. P.; Lai, K.; Fujii, N.; French, S.; Xu, J.; Wang, J. Y.; Murali, R.; Mishra, L.; Lee, J. S.; Ntambi, J. M.; Tsukamoto, H. Stearoyl-CoA Desaturase Promotes Liver Fibrosis and Tumor Development in Mice via a Wnt Positive-Signaling Loop by Stabilization of Low-Density Lipoprotein-Receptor-Related Proteins 5 and 6. *Gastroenterology* **2017**, *152* (6), 1477−1491.
(33) Bekric, D.; Ocker, M.; Mayr, C.; Stintzing, S.; Ritter, M.; Kiesslich, T.; Neureiter, D. ferroptosis in Hepatocellular Carcinoma: Mechanisms, Drug Targets and Approaches to Clinical Translation. *Cancers* **2022**, *14* (7), 1826 DOI: 10.3390/cancers14071826.
(34) Li, L.; Wang, K.; Jia, R.; Xie, J.; Ma, L.; Hao, Z.; Zhang, W.; Mo, J.; Ren, F. Ferroportin-dependent ferroptosis induced by ellagic acid retards liver fibrosis by impairing the SNARE complexes formation. *Redox biology* **2022**, *56*, No. 102435.

https://doi.org/10.1021/acs.jafc.3c03409
J. Agric. Food Chem. 2023, 71, 17295−17307